



Measurement and Simulation of Transverse Emittance Growth along the Alvarez DTL of the GSI UNILAC

L. Groening¹, W. Barth¹, W. Bayer¹, L. Dahl¹, P. Forck¹, P. Gerhard¹, I. Hofmann¹, G. Riehl¹,
S. Yaramyshev¹, D. Jeon²,

1) GSI, Darmstadt, Germany

2) Oak Ridge National Laboratory, Oak Ridge, U.S.A.

Abstract

Transverse emittance growth along the Alvarez DTL section is a major concern with respect to the preservation of beam quality of high current beams at the GSI UNILAC. In order to define measures to reduce this growth appropriated tools to simulate the beam dynamics are indispensable. This note is about the benchmarking of two beam dynamics simulation codes, i.e. DYNAMION and PARMILA, against systematic measurements of beam emittances for different machine settings. Experimental set-ups, data reduction, the preparation of the simulations, and the evaluation of the simulations will be described. It was found that the measured 100%-rms-emittances exceed the simulated values. Comparing measured 90%-rms-emittances with the simulated 95%-rms-emittances gives fair to good agreement instead. The sum of horizontal and vertical emittances is even described well by the codes as long as experimental 90%-rms-emittances and simulated 95%-rms-emittances are compared.

1 Introduction

At GSI currently the new Facility for Antiproton and Ion Research (FAIR) is under design [1]. It comprises two new superconducting synchrotrons and five storage rings to provide radioactive beams and exotic nuclei. The existing GSI facility will serve as an injector chain for FAIR and hence must deliver the primary beam intensities. It comprises the UNiversal Linear ACcelerator (UNILAC), the heavy ion synchrotron SIS, and an experimental storage ring.

The UNILAC [2] can accelerate ions from protons to uranium (Fig. 1.1). Beams from three different ion sources can be delivered to various experiments or to the SIS18 in pulse-switching mode. Its initial design from the late 1960ies did not foresee the high intensity operation where space charge forces need to be considered in the beam dynamics layout. However, the UNILAC underwent several upgrades [2] and since 1999 many experiments have been served successfully with high intensity beams.

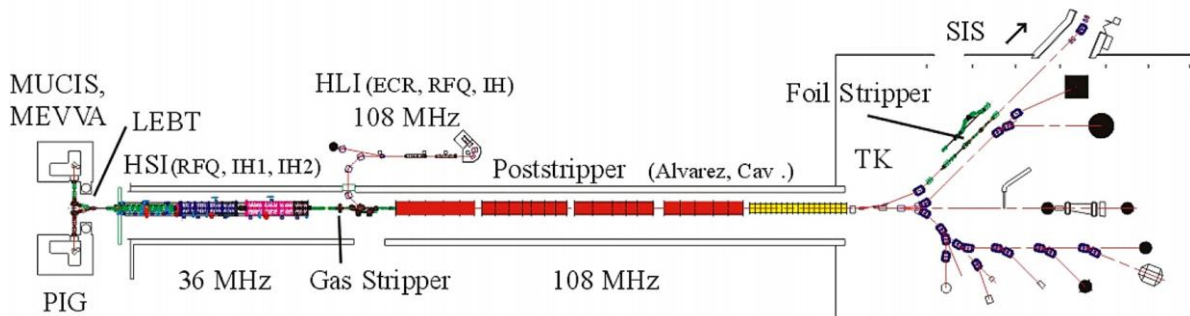


Figure 1.1: The UNiversal Linear ACcelerator UNILAC at GSI.

With the upcoming FAIR project the demands on high intensity beams to the UNILAC increased. The FAIR physics program especially asks for intense beams of uranium pre-accelerated by the UNILAC to 11.4 MeV/u before injection into the SIS. Intense uranium beams are provided by a MEVVA source at charge state 4+ and with the energy of 2.2 keV/u. An RFQ followed by two IH-cavities (HSI section) accelerates the ions to 1.4 MeV/u using an rf-frequency of 36 MHz. A subsequent gas-stripper increases the average charge state to 28+. Final acceleration to 11.4 MeV/u is done in the Alvarez-DTL section operated at 108 MHz. The increase of rf-frequency by a factor of three requires a dedicated matching section preceding the DTL as shown in Fig. 1.2.

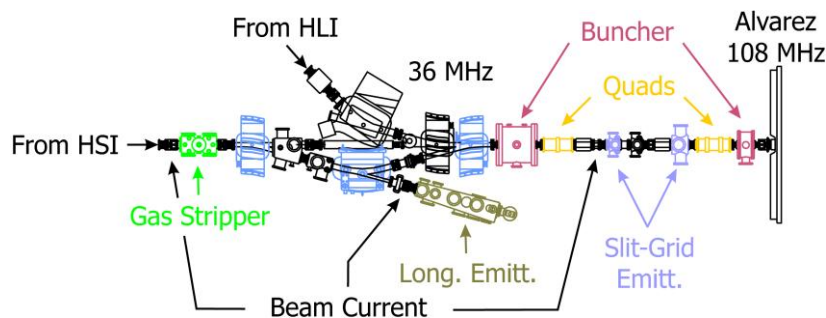


Figure 1.2: The stripper section including the matching section to the Alvarez DTL.

It comprises a 36 MHz buncher for longitudinal bunch compression, a 108 MHz buncher for final bunch rotation, a quadrupole duplet for transverse compression, and a quadrupole triplet for final transverse beam matching.

The Alvarez DTL consists of five independent rf-tanks accelerating to 3.6, 4.8, 5.9, 8.6, and 11.4 MeV/u, respectively. Transverse beam focusing is done by quadrupoles in the F-D-D-F mode. Each drift tube houses one quadrupole. The periodicity of the lattice is interrupted in the four inter-tank sections, where D-F-D focusing is applied. Acceleration takes place -30° from crest in the first three tanks and -25° from crest in the last two tanks. Different beam energies behind the DTL are available by switching off the acceleration in the last tanks. However, the production mode for FAIR foresees full acceleration to 11.4 MeV/u with the design beam parameters as summarized in Tab. 1.1. The DTL is followed by a section of ten single gap resonators for energy variation behind the DTL. They have not been used for the experiments described here.

Table 1.1: Design beam parameters of the UNILAC for uranium as required by FAIR.

	RFQ Entrance	DTL Entrance	SIS Injection
Ion species	$^{238}\text{U}^{4+}$	$^{238}\text{U}^{28+}$	$^{238}\text{U}^{28+}$
Current [emA]	18	15	15
Energy [MeV/u]	0.002	1.39	11.4
Energy Spread	-	$\pm 1 \cdot 10^{-2}$	$\pm 2 \cdot 10^{-3}$
$\beta\gamma\epsilon_{\perp}$ (tot, norm) [mm mrad]	0.3	0.75	1.1

Injection into the synchrotron SIS is done using horizontal multi-turn-injection. This scheme imposes an upper limit for the horizontal emittance at the injection point thus reducing the budget for eventual emittance growth during beam acceleration and transportation. Previous beam experiments showed transverse growth rates of up to a factor of five just along the DTL section at high currents. In order to reduce this growth, its course has to be investigated experimentally accompanied by beam dynamics simulations.

However, any hardware measure to reduce the growth should be checked by simulations before being implemented into the real machine. This step is based on the reliability of the respective simulation code, or put with other words, on the knowledge of the limits of the applied code. In order to clarify better the last two issues a benchmark activity had been integrated into the CARE-JRA "HIPPI". It aims for the simulation of systematic beam emittance measurements performed at the DTL-entrance and -exit, respectively.

Previous simulations [3] indicate that for mismatched injection into the DTL emittance growth mainly occurs at the low energy end of the DTL where space charge forces are stronger. The experimental campaign described in Chap. 3 addresses this issue.

At measurements with $^{238}\text{U}^{28+}$ it had been observed that the transverse growth decreases with the transverse phase advance imposed by the DTL quadrupoles [3]. The encouraging findings of these measurements called for a more detailed experimental investigation of the dependence of emittance growth on transverse focusing strength. Chapter 4 deals with the respective experiment and the simulations. Due to the large mass over charge ratio of this ion, the maximum zero current phase advance σ_0 that can be applied along the DTL is 54° . Additionally, the maximum current achieved so far with $^{238}\text{U}^{28+}$ had been 5.5 emA at the DTL entrance thus not providing the space charge conditions at the design current of 15 emA.

The two limitations could be removed by using a $^{40}\text{Ar}^{10+}$ beam which can be delivered with currents of more than 10 emA at the DTL entrance. The maximum σ_0 applicable to $^{40}\text{Ar}^{10+}$ exceeds 180° . In order to estimate the relevance of space charge forces at a given location along the DTL, the value $I \cdot q/A$ for the specific ion must be calculated, where I is the electric beam current, q is its charge state, and A is its mass number. The application of this rule shows that a 7.1 emA beam of a $^{40}\text{Ar}^{10+}$ is space charge equivalent to a 15 emA beam of $^{238}\text{U}^{28+}$. Table 2.1 summarises the parameter variations of the two benchmarking campaigns.

Table 2.1: Parameters of the two benchmarking campaigns.

	Campaign 2005 Chapter 3	Campaign 2006 Chapter 4
Ion	$^{40}\text{Ar}^{10+}$	
Mean pulse current [emA]	9.5 emA	7.1 emA
Final DTL energy [MeV/u]	3.6, 4.8, 5.9, 8.6, 11.4	11.4
σ_0 [deg]	53	35, 40, 45,, 85, 90
Simulation codes	DYNAMION	DYNAMION, PARMILA
Starting point for simulations	entrance to DTL	entrance to 36 MHz buncher

2 Experiment set-up

Figure 2.1 shows the schematic set-up of the experiments. A high current beam of $^{40}\text{Ar}^{1+}$ is delivered from the HSI and passed through the gas stripper. The subsequent 3-dipole chicane in connection with horizontal scrapers filters the desired charge state of 10+. The variable gas density of the stripper is a tool to vary the current within the selected charge state preserving the phase space area being occupied by the ions, i.e. the beam current can be set while the emittances remain unchanged.

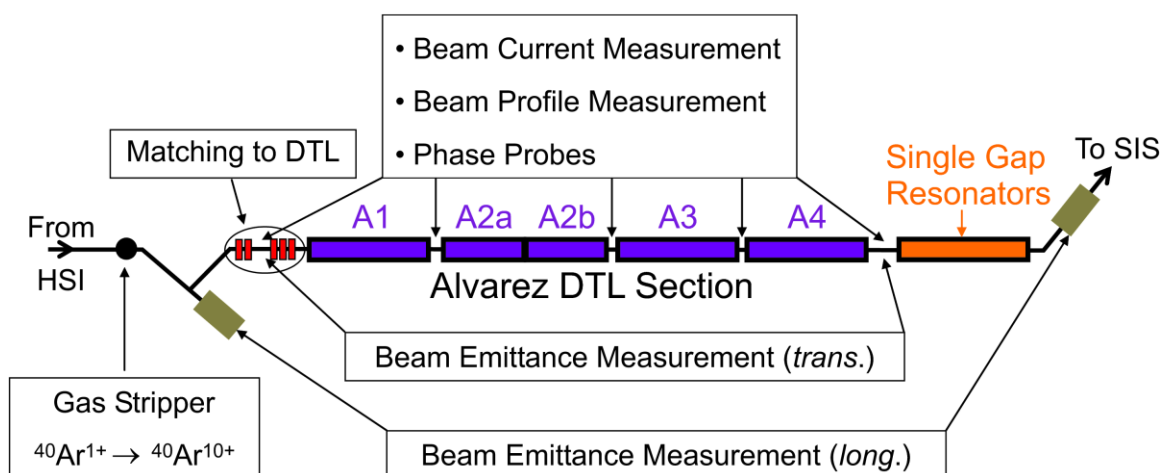


Figure 2.1: Schematic set-up of the experiments.

One beam current transformer is placed before the DTL between the quadrupole doublet and triplet. Additional transformers are located after the tanks A1, A2b, A3, and A4. They were used to measure the input current and the beam transmission along the DTL. Horizontal and vertical profile grids are located before the first tank and behind each of the five Alvarez tanks. The ones before and behind the DTL are preceded by horizontal and vertical slits and used as transverse emittance measurement units. To measure one plane takes about five minutes with a resolution of 1mm in space and 0.5 mrad in angle. During the measurement time several 10^5 bunches impact on the measurement device, thus the final result will represent the averaged emittance of the bunch train.

A set-up to measure the longitudinal emittance is available in front of the DTL [4]. It measures the arrival time of single ions on a foil with respect to an rf-reference at 36 MHz, followed by a time-of-flight measurement for the ions. From these two measurements the ions positions within the bunch and their energy can be extracted. A second system is installed in a dispersive section behind the DTL. It comprises an iris for transverse emittance reduction, a vertical buncher operated at 108 MHz, a focusing doublet, and transverse profile grids. The dispersion transforms the energy deviation into horizontal displacement, while the buncher transforms the longitudinal off-centre position into a vertical displacement. The preceding iris and the doublet minimize the intrinsic transverse beam dimensions. If the grids are replaced by a fluorescence screen, the set-up can be used as an online tool to display the longitudinal phase space distribution. It had been used to reduce low energy beam tails at the DTL exit. The extension of the set-up towards a tool for quantitative longitudinal emittance measurements is still ongoing.

The experiments described in the subsequent chapters were performed in March 2005 and in December 2006. In order to prepare the corresponding simulations different methods were used. In addition, during the simulation of the 2006 campaign also the matching section preceding the DTL has been included into the simulations.

3 Transverse emittances as function of the final energy at the DTL exit (Campaign 2005)

As mentioned in Chap. 1 for mismatched DTL injection the main part of the transverse emittance growth along the DTL was expected to occur at the low energy end. Since the space in the inter-tank section is limited, emittances cannot be measured there. The next measurement set-up is located behind the complete DTL. To measure the emittances between tanks another approach had been followed. It is based on the assumption that transverse emittance growth just occurs when longitudinal beam focusing is applied. Without this focusing the de-bunching will reduce the space charge forces rapidly and cut the growth. Before the experiments this assumption was tested by DYNAMION [5] simulations based on design values for the input emittances. A 12.5 emA beam of $^{238}\text{U}^{28+}$ was injected rms-matched into the Alvarez DTL set to a zero current phase advance σ_0 of 50° . The beam rms-emittances are plotted against the position along the beam line as shown in Fig. 3.1. Simulations had were for four different cases:

1. all five tanks rf-powered
2. just the first four tanks rf-powered
3. just the first three tanks rf-powered
4. just the first two tanks rf-powered.

Although the rf-power for some of the tanks was switched off, the quadrupole gradients in these tanks remained unchanged, resulting in an increase of the transverse phase advance along the DTL.

The loss-free simulations confirmed that transverse emittance growth stops when the beam bunches are not rf-focused any longer [6]. Accordingly, the transverse emittance behind a given tank can be measured also behind the complete DTL as long as no rf is applied to those tanks behind the specific tank of interest. The results also show that the emittance growth at the DTL entrance could be completely suppressed by proper rms-matched injection into the DTL. However, this rms-matched injection could not have been applied during the experiments due to missing information on the longitudinal emittance as to be addressed in Chap. 4.

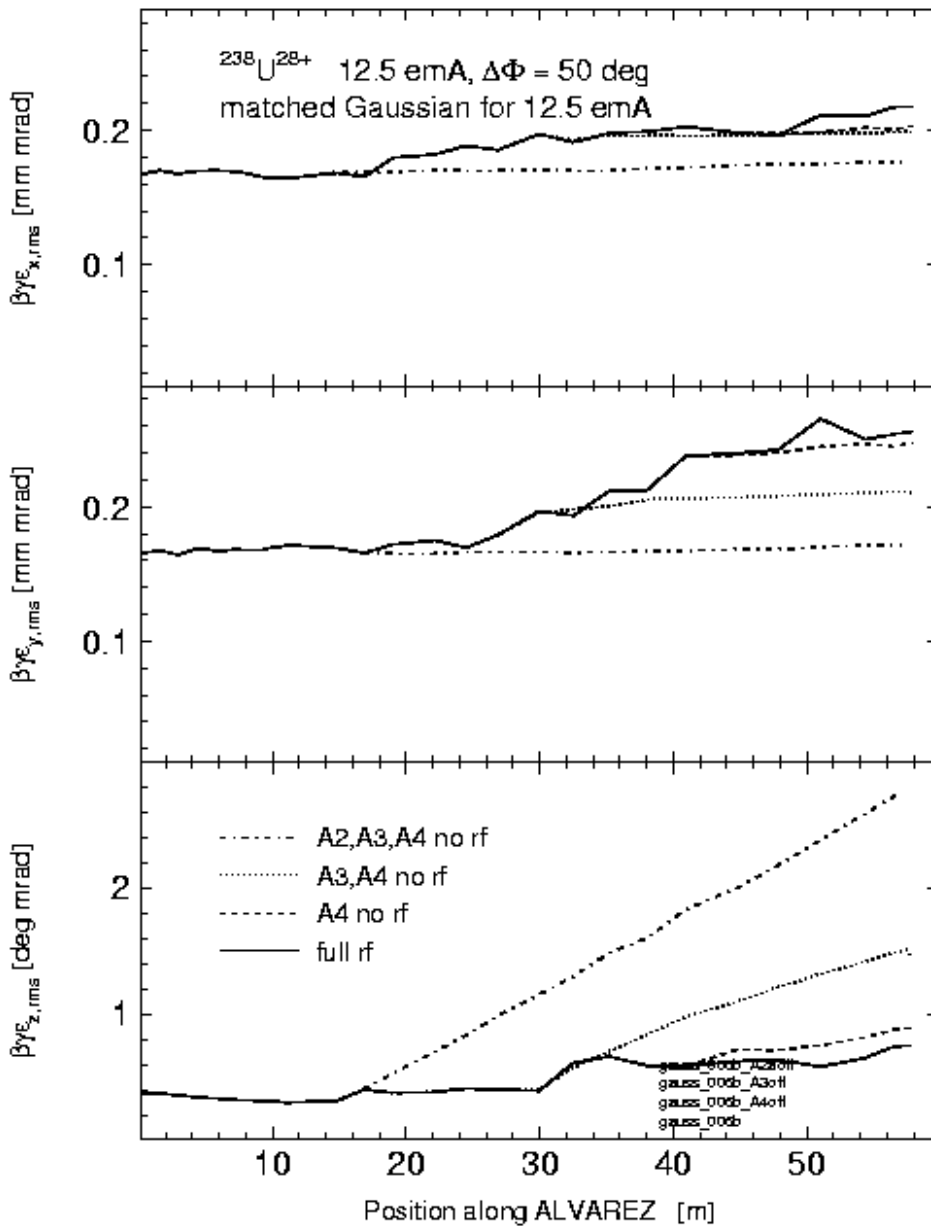


Figure 3.1: DYNAMION simulations of rms-emittance growth along the Alvarez DTL for different final energies at the DTL exit. Energy variation is accomplished by switching off the rf-power in some tanks.

3.1 Experimental procedure

The experiments were performed in March of 2005 with an intense $^{40}\text{Ar}^{1+}$ beam from the HSI at 1.4 MeV/u. The gas stripper was set to obtain 9.5 emA of $^{40}\text{Ar}^{10+}$ in front of the DTL. Along the DTL a zero current phase advance σ_0 of 53° was applied resulting in a real phase advance σ of 24° due to space charge tune depression of 55%. The matching section (Fig. 1.2) was set manually to almost full transmission (96%) through the fully rf-powered Alvarez DTL. Beam transformers along the dispersive section in the transfer section towards the SIS18 together with horizontal profile grids were used to minimize low energy tails behind the DTL. Such tails indicate longitudinally mismatched injection into the first Alvarez tank. They can be minimized by fine-tuning of the IH-cavities in the HSI and of the two bunchers in front of the DTL. After this optimization the tails contain less than a percent of the total beam current.

In the next step the transverse beam emittances at the DTL entrance and at the DTL exit are measured. The first emittance measurement behind the exit has been done at the full energy of 11.4 MeV/u, i.e. all five tanks were rf-powered.

Afterwards the rf-power of the last tank was switched off resulting in a final DTL energy of 8.6 MeV/u. The quadrupole settings remained unchanged and the 96% DTL transmission was kept without any intervention. Due to the different transverse focusing (lower beam energy!) in the last tank, the strength of the doublet behind the DTL had to be adjusted in order to assure the measurement of the complete beam emittances with the slit/grid set-up.

The same procedure was applied for the cases where the other tanks were driven without rf, i.e. at beam energies at the DTL exit of 5.9, 4.8, and 3.6 MeV. Transmission was kept always at 96% except for the 3.6 MeV/u case where it dropped to 83%. The losses were due to the very large transverse betatron oscillations of the low energy beam in the last DTL tanks. Reducing the quad strength could have preserved the transmission but the strict time boundaries for doing the experiments did not allow for that. Finally the transverse emittances at the DTL entrance had been re-measured to verify that the initial beam conditions did not change during the experiment.

3.2 Data reduction

Each emittance measurement delivers a two dimensional matrix of discrete slit-positions and discrete angles. To each element of the matrix a value is appointed that corresponds to the density of phase space population at this phase space coordinate (pixel). The raw data are displayed by the measurement & evaluation program PROEMI. Data reduction is done in three steps as shown in Fig. 3.2.

For the used set-up the noise comprises two components: a first homogenous one that scatters all over the scanned phase space area, and a second one being located around the beam centre and expanding over the full range of angles homogeneously. By cutting the measured distribution horizontally, i.e., reducing the content of all pixels by the same amount, the first contribution of the noise is eliminated. The second component is cut by setting to zero the content of all pixels that are still affected by noise after the first horizontal cut.

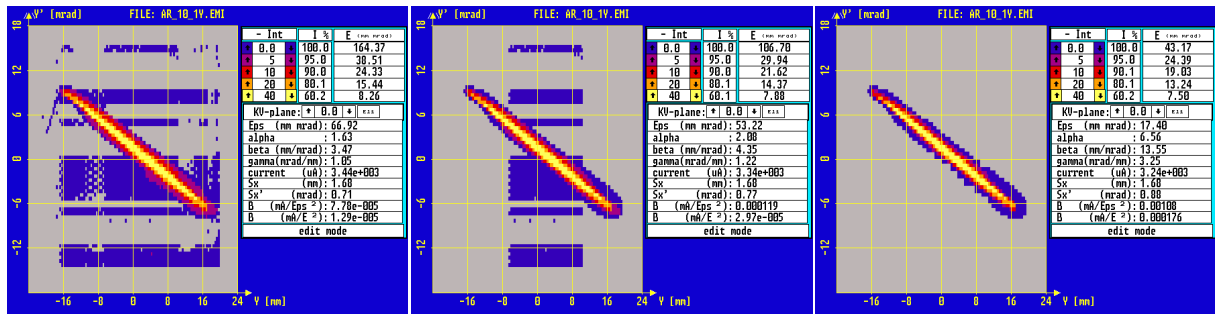


Figure 3.2: Elimination of noise from the experimental data. Left: raw data; centre: homogeneous noise is cut; right: remaining signals not related to beam are cut.

For the remaining distribution the 100%-rms-emittance is calculated considering the statistical weight of each pixel which is proportional to the pixel content. Alternatively, fractional emittances can be extracted from the remaining distribution as well. This is useful for distributions that are not homogeneous and where the Twiss parameters of a dense core are considerably different from those of the full distribution. In practical cases it is beneficial to adopt the focusing to the "inner" 90% of the particles instead of putting huge efforts to achieve an optic that fits to the 100% Twiss parameters. The emittance containing X% of the full distribution is extracted as follows:

1. The sum S100 of all pixel contents is calculated
2. The pixels are sorted by their content starting with the highest
3. Starting from the highest content the sum of all pixel contents is built as long as this sum is less or equal to X% of S100.
4. Those pixels that contributed to the sum are considered for the rms-evaluation. The content of the others is omitted.

Figure 3.3 shows the result of the evaluation of a 100%, 95%, and 90%-rms-emittance and the corresponding Twiss parameters. The total accuracy of each emittance measurement including its evaluation is estimated to be 10%.

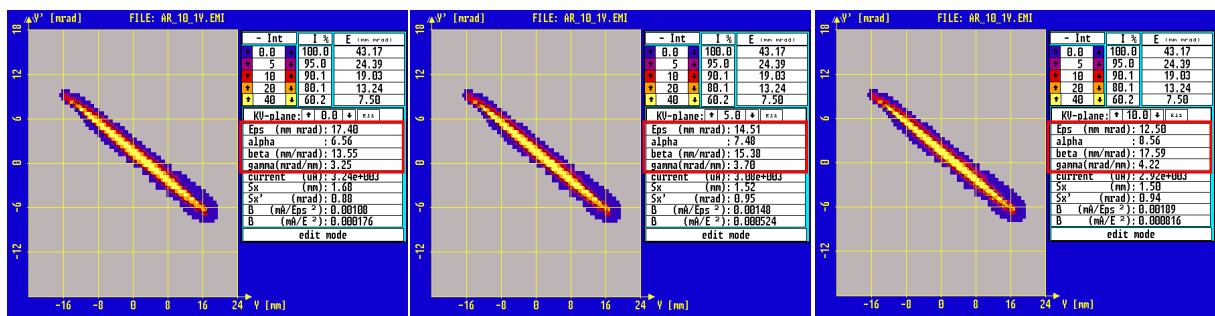


Figure 3.3: Fractional 4-rms-emittances and rms-Twiss parameters (highlighted in red): Left 100%; centre: 95%; right: 90% (percentages with respect to full intensity).

3.3 Preparation of input for simulations

From the transverse emittances as measured in front (see Fig. 1.2) of the DTL normalized 90%-rms-emittances of 0.16 and 0.17 mm rad were extracted horizontally and vertically, as shown in Fig. 3.4. These values for the 90%-rms-emittances were chosen for the 100%-rms-emittances of the distributions for the DYNAMION simulations using 1500 particles and 3D-particle-particle interaction. During the first campaign (March 2005) it was assumed that the missing 10% are still due to residual noise of the experiment and that they should not enter into the simulations.

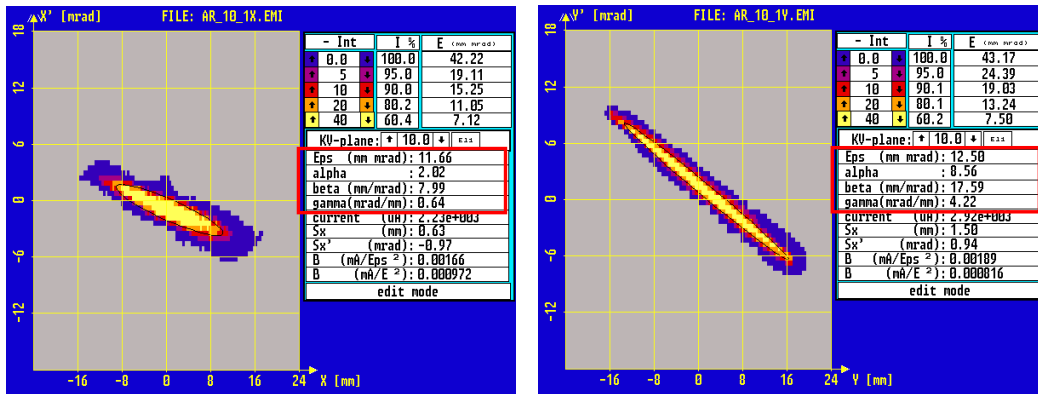


Figure 3.4: Horizontal and vertical phase space distributions measured in front of the DTL for a 9.5 emA beam of $^{40}\text{Ar}^{10+}$. The rms-Twiss parameters corresponding to 90% of the total intensity are highlighted in red.

Since longitudinal emittance measurements were not done in 2005, the design value of 7 deg mrad was assumed for the 100%-rms-emittance (referring to relative momentum spread and phase spread at 108 MHz). The simulations started right at the first accelerating gap of the DTL. In 2005 the values for rms-matched injection for zero current were assumed for the beta-functions and alpha-parameters. As distribution type a Gaussian cut at 2σ was chosen. Figure 3.5 presents the corresponding phase space distribution assumed for the simulations. Since the locations of the emittance measurement set-up and of the starting point of the simulations are different, the orientations of the ellipses differ as well.

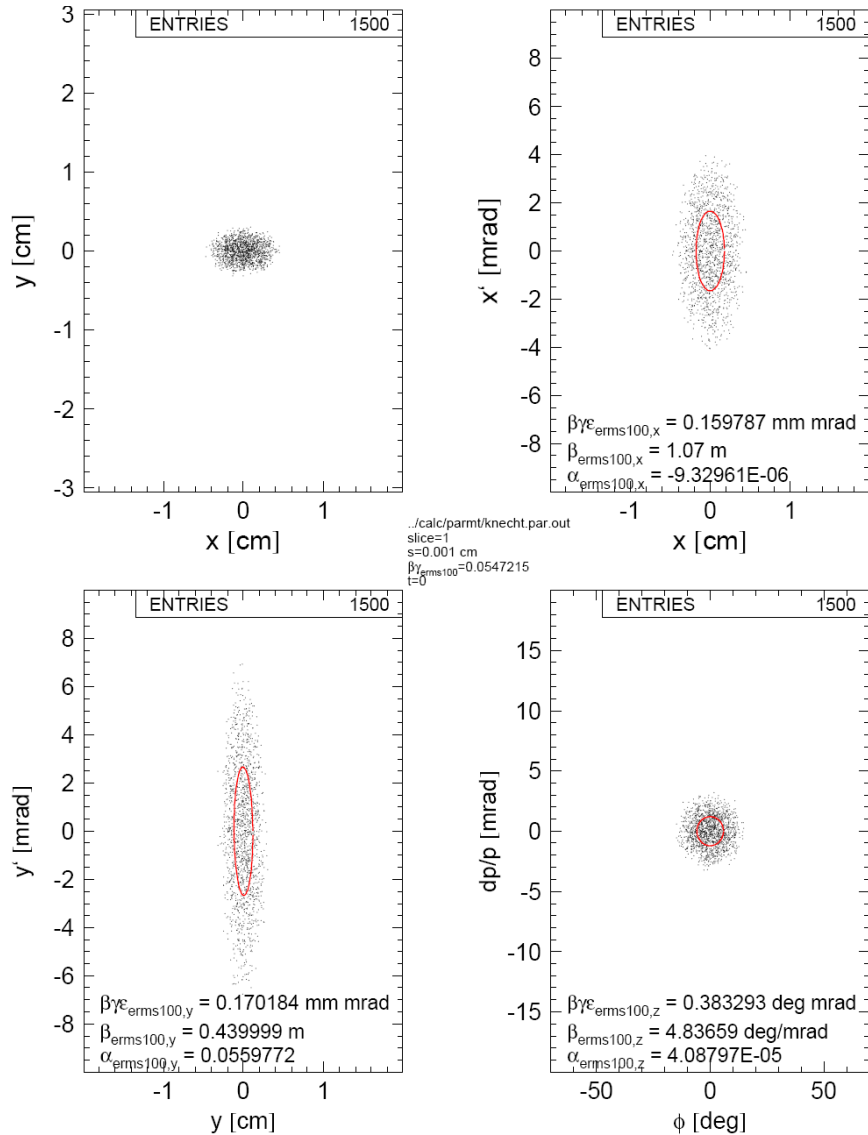


Figure 3.5: Initial phase space distribution for the DYNAMION simulations of the 2005 benchmarking campaign. The 100%-rms-ellipses are drawn in red and the corresponding rms-Twiss parameters are listed.

3.4 Evaluation of simulation results

In order to compare the results of measurements and simulations adequately it must be assured that the simulated emittances are defined in the same way as their experimental pendants. This applies especially for the evaluation of fractional emittances from simulations. A simulation delivers a set of 6-dimensional particle coordinates. This ensemble is projected onto a pixel-grid having the same characteristics as the slit/grid device used for the measurements. The obtained matrix is written into a file using the same format as the files containing measured phase space data. Accordingly, the file is put into the measurement evaluation program PROEMI such that data reduction is done in the same way as for measured data (Chap. 3.2). Figure 3.6 depicts this transformation of format. It displays the vertical phase space distribution of a simulation for a 9.5 eA $^{40}\text{Ar}^{10+}$ beam fully accelerated in the DTL and evaluated at the exit of the DTL.

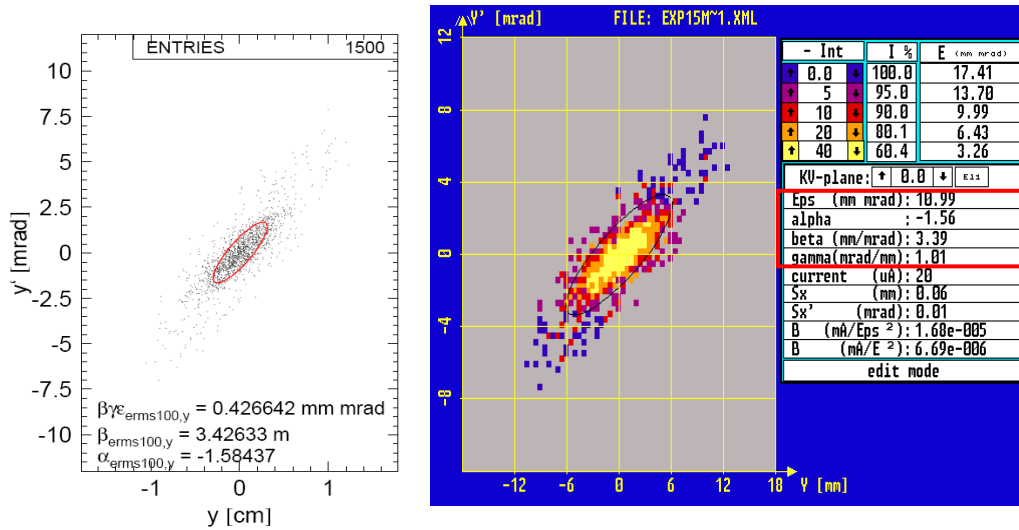


Figure 3.6: Transformation of the format of a distribution from a DYNAMION simulation (left) into a format of measured data (right). The 100%-rms-Twiss parameters are highlighted in red. PROEMI (right) displays the rms-emittance value times four. The normalization factor is $\beta\gamma = 0.157$.

3.5 Comparison of experimental data and simulation results

In the experiments full beam transmission was achieved for all settings except the 3.6 MeV/u case where it dropped to 83%. The simulations gave 98% for 3.6 MeV/u and full transmission at all higher final energies.

Fig. 3.7 depicts the horizontal phase space distributions behind the DTL measured (upper) and simulated (lower) for two different final energies. The left side shows the case for acceleration just in the first three tanks, i.e. to 5.9 MeV/u, while on the right side the case for full acceleration to 11.4 MeV/u is shown. Highlighted in red are the evaluated Twiss parameters.

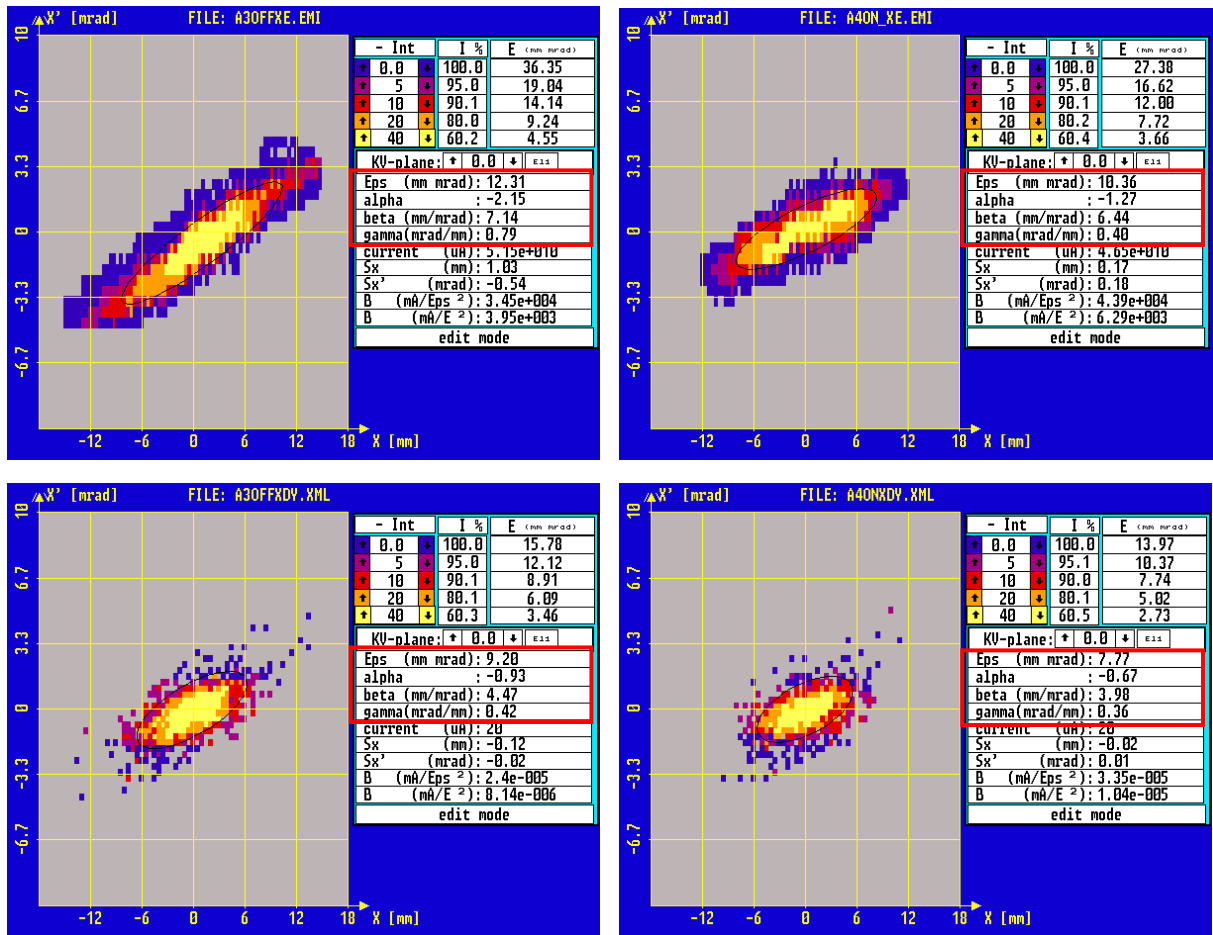


Figure 3.7: Measured (top) and DYNAMION-simulated (bottom) horizontal phase space distributions at the DTL exit for a final beam energy of 5.9 MeV/u (left) and 11.4 MeV/u (right).

3.5.1 Comparison of 100%-rms-emittance data

From the experimental data and the DYNAMION-simulated data the 100%-rms-emittances have been extracted, i.e. the full intensity has been taken into account for the evaluation. The resulting horizontal and vertical rms-emittances as function of the final DTL energy are plotted in Fig. 3.8a. Averaged transverse emittances, i.e. the mean values of horizontal and vertical emittances, are presented in Fig. 3.8b.

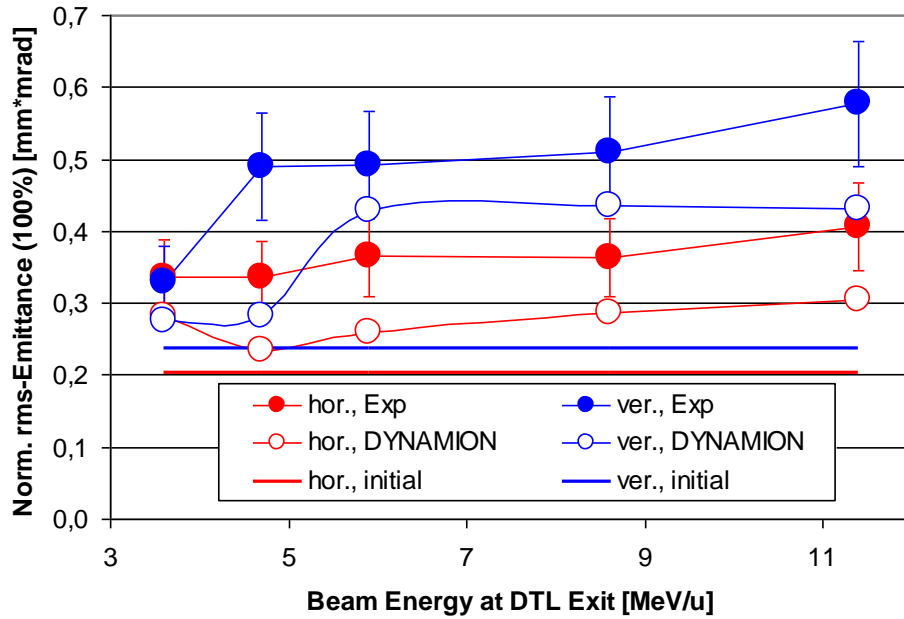


Figure 3.8a: Horizontal and vertical 100%-rms-emittances at the DTL exit as function of the final DTL energy.

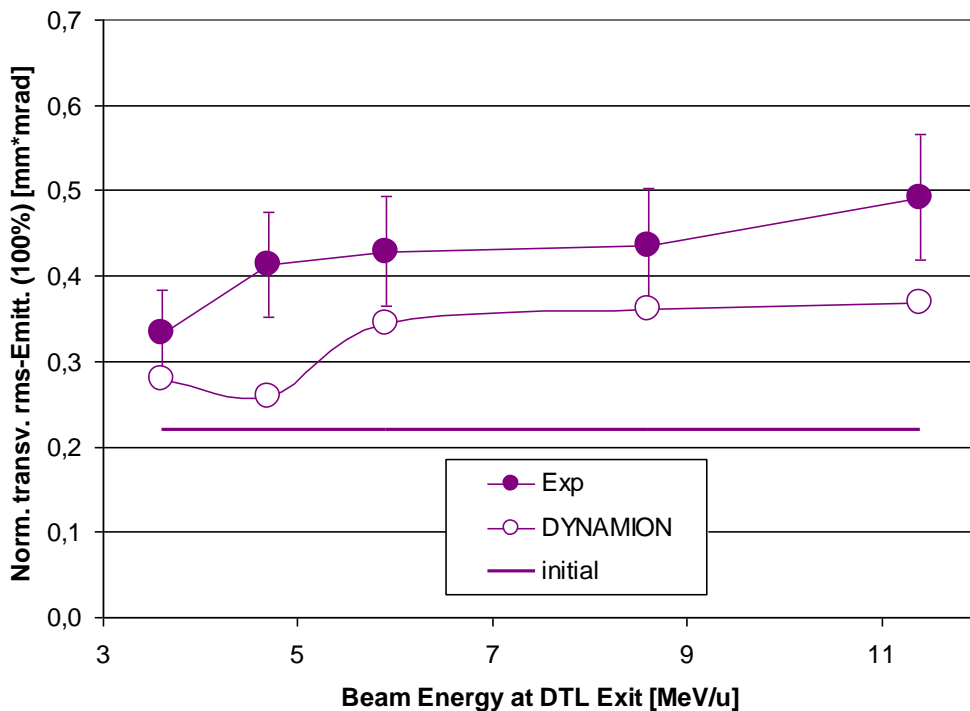


Figure 3.8b: Mean value of horizontal and vertical 100%-rms-emittances at the DTL exit as function of the final DTL energy.

In the experiment and in the simulations the vertical emittances are larger than the horizontal ones. The vertical increase of the emittance occurs mainly at the low energy end of the DTL. Generally, the measured 100%-emittances are larger than the simulated ones. However, the

measurement gives the averaged emittances of several 10^5 bunches, while a simulation evaluates just a single bunch ignoring a possible jitter in bunch current or rf-phase and amplitude. Furthermore each "experimental" bunch includes $1.6 \cdot 10^8$ ions and the DYNAMION-simulation employed just 1500 particles which might not adequately represent the space charge effects. Future experiments aim for the dependence of the 100%-rms-emittance on the number of bunches contributing to one measurement. Another explanation for the observed difference between experimental and simulated 100%-rms-emittances might be given by the fact that the simulations neglect any kind of machine error. Errors like quadrupole positioning, gap-voltage and rf-phase jitters contribute to emittance increase in all three dimensions. These errors are intrinsically imposed by finite machining tolerances and by noise in rf-amplifier operation.

The effect of cross-talking profile grid wires due to electrons released during the impact of ions on the wire results in a widening of the measured angular profiles. Its strength was estimated to be just a few percent of growth of the measured emittance with respect to the real emittance. Accordingly, this effect is too weak to explain the observed differences between measured and simulated 100%-rms-emittances.

3.5.2 Comparison of measured 90%-rms-emittance data with simulated 95%-rms-emittances

Generally in laboratory reports or publications fractional emittances are stated. Given emittance values refer to a fraction of $\geq 90\%$ of the overall current or number of particles as result of measurements or simulations.

In case of previous measurements done at the UNILAC, for instance, measured 90%-rms-emittances had been referred to. Simulations in turn often refer to fractional emittances in order to eliminate the influence of individual particles with high single particle emittances. Fractional emittances in this report are defined as described in Chap. 3.4.

While the previous chapter compared the 100%-rms-values of experiments and simulations, this chapter benchmarks the experimental 90%-rms-values with the simulated 95%-rms-values. There is partial arbitrariness in choosing these values, since also other fractions could have served for doing that. However, the two fractions should not be less than 90% in order to extract the information from the major part of the beam. Additionally, the fractions should be less than 100% for the reasons stated before, and finally, the simulated fraction might be chosen to be larger than its experimental pendant due to the large difference in number of particles and bunches comprising an experiment and a simulation, respectively.

A comparison of measured 90%-rms-emittances with simulated 95%-rms-emittances is presented in Fig. 3.9. In Fig. 3.9a the horizontal and vertical emittances are plotted separately, and in Fig. 12b the averaged transverse emittance, i.e. the mean of horizontal and vertical emittances, is plotted.

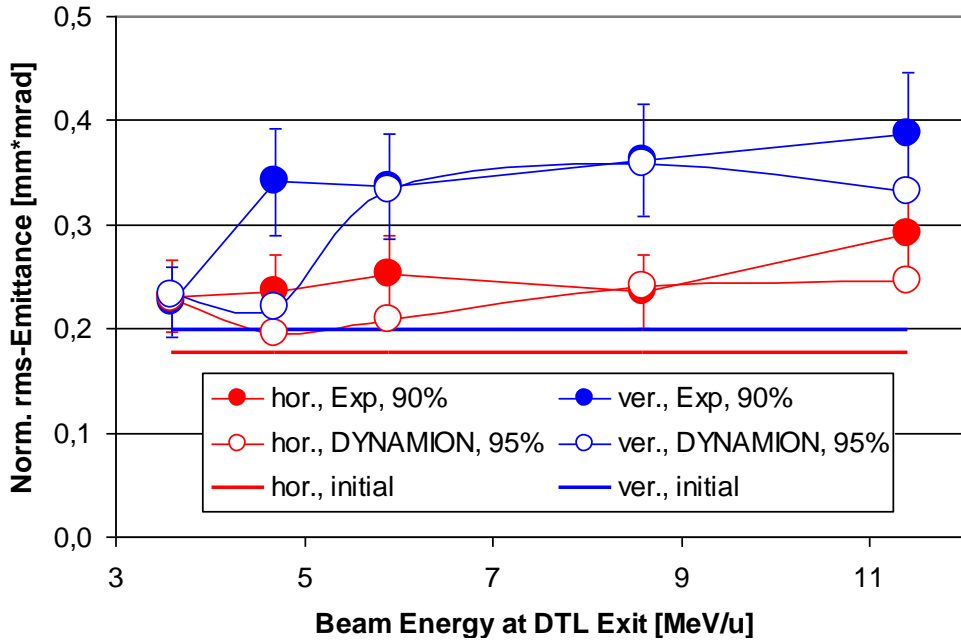


Figure 3.9a: Horizontal and vertical rms-emittances at the DTL exit as function of the final DTL energy. The experimental values refer to 90% of the total intensity while the simulated values refer to 95% of the particles.

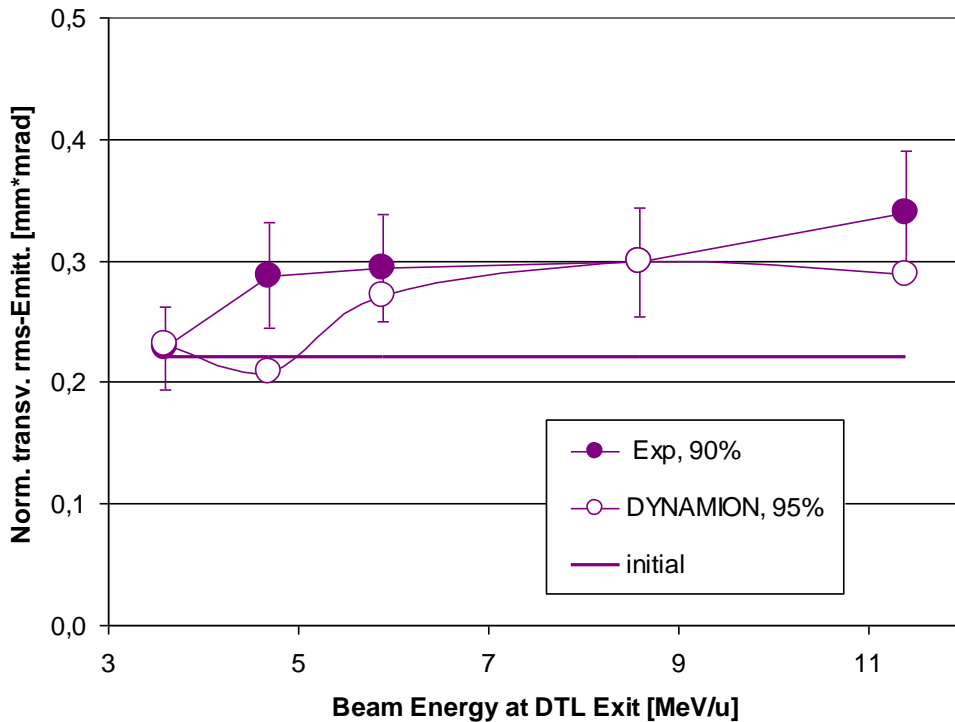


Figure 3.9b: Mean value of horizontal and vertical rms-emittances at the DTL exit as function of the final DTL energy. The experimental values refer to 90% of the total intensity while the simulated values refer to 95% of the particles.

With exception of the vertical emittance at 4.8 MeV/u all simulated emittance values are within the estimated error bars of the measurements. Horizontal and vertical emittances are described well by the DYNAMION simulation, respectively. However, for the 3.6 MeV/u case the measured (83%) and simulated transmission (98%) differed considerably such that the corresponding emittance values should not be compared in a straight forward way.

4 Transverse emittances as function of the quadrupole focussing strength along the DTL (Campaign 2006)

During the second experimental campaign in December 2006 the emittance growth was investigated as function of the transverse focusing strength along the DTL. All Alvarez tanks were rf-powered such that the final DTL energy was 11.4 MeV/u. The focussing strength is quantified by the transverse phase advance σ_0 being imposed to a beam of very low intensity such that no space charge forces are present. For non-vanishing beam currents this zero current phase advance σ_0 is depressed due to the defocusing sign of space charge forces to the actual phase advance σ .

4.1 Experimental procedure

As in the 2005 campaign (Chap. 3.1) the $^{40}\text{Ar}^{10+}$ beam of 7.1 emA was prepared in front of the DTL. Transverse emittances were measured in front of the DTL as presented in Fig. 4.1.

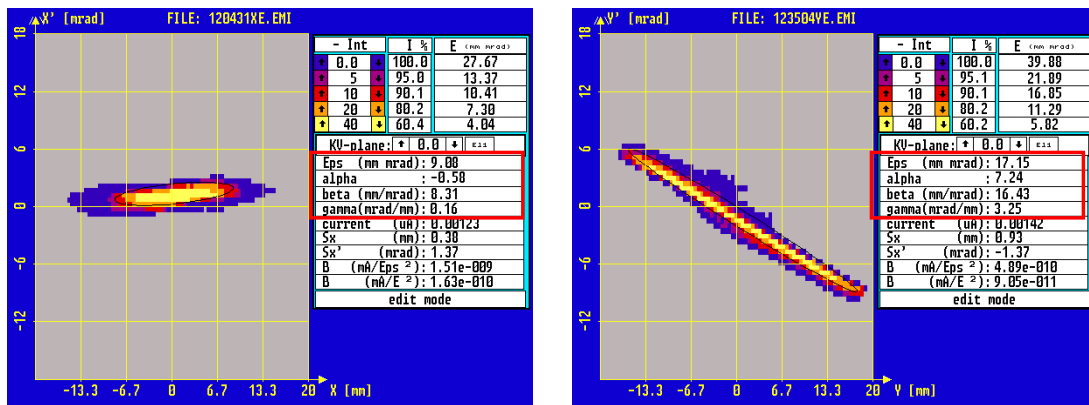


Figure 4.1: Horizontal and vertical phase space distributions measured in front of the DTL for a 7.1 emA beam of $^{40}\text{Ar}^{10+}$. The rms-Twiss parameters corresponding to 100% of the total intensity are highlighted in red.

Additionally, the set-up for longitudinal emittance measurements [4] (Fig. 2.1) was used to measure the longitudinal phase space distribution in front of the DTL (Fig. 4.2). Although the absolute rms-bunch length seemed reasonable, the measurement suggested an uncorrelated longitudinal phase space distribution. Taking into account that the last rf-focusing was applied about 15 m in front of the set-up, a strongly divergent distribution ought to have been measured instead.

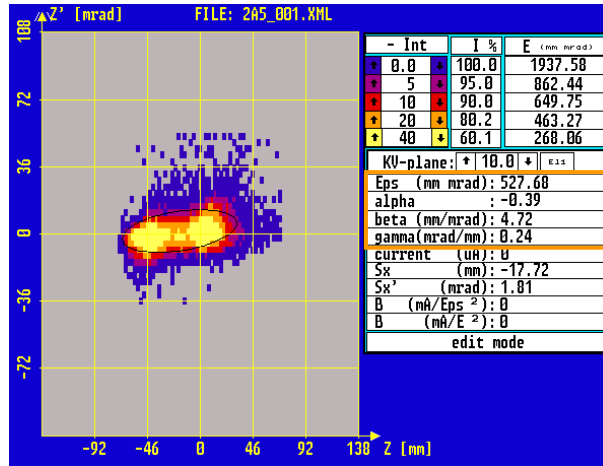


Figure 4.2: Measurement of the longitudinal phase space distribution before the DTL. See text for further explanations. The measured value of alpha close to zero seems unrealistic.

The DTL was set to different phase advances σ_0 ranging from 35° to 90° in steps of 5° . Due to the defocusing space charge forces the phase advances in all three dimensions were depressed as listed in Tab. 4.1.

Table 4.1: Horizontal, vertical, and longitudinal phase advances along the DTL in case of zero current (left) and of 7.1 emA of $^{40}\text{Ar}^{10+}$ (right) for an rms-equivalent KV-beam.

σ_0 [deg]			σ [deg]		
horizontal	vertical	longitudinal	horizontal	vertical	longitudinal
35	35	43	18	22	39
40	40	43	22	27	39
45	45	43	26	31	39
50	50	43	31	36	38
55	55	43	35	41	38
60	60	43	40	45	38
65	65	43	44	50	37
70	70	43	49	55	37
75	75	43	54	60	37
80	80	43	58	64	37
85	85	43	63	69	37
90	90	43	68	74	36

For each setting the section in front of the DTL was set in order to rms-match the beam into the DTL. A dedicated rms-matching routine was established for that as described in [7]. Unfortunately during the experiments it was not realized that the measured longitudinal Twiss parameters were not realistic, and they have been used anyway as input for the matching routine. *(This circumstance for sure was compromising with respect to successful rms-matching into the DTL. However, it did not affect the intention of the benchmarking campaign, i.e. the comparison of measured and simulated emittances.)*

After setting the desired σ_0 along the DTL the quadrupoles preceding the DTL were set as suggested by the rms-matching routine. The suggested buncher settings were not applied. Instead the manually found buncher settings were kept for all values of σ_0 . Applying this

procedure full DTL transmission was achieved for all zero current phase advances ranging from 35° to 90° . For all values of σ_0 horizontal and vertical beam emittances were measured behind the DTL. The measurements have been evaluated in the same way as mentioned in Chap. 3.2.

In order to check the reproducibility of these measurements seven settings of σ_0 were measured twice. The observed differences between two measurements using the same settings were just a few percent with respect to rms-emittances.

After the full σ_0 scan the initial emittances in front of the DTL were re-measured in both transverse planes and longitudinally. The measured shapes of the distributions confirmed that the initial beam conditions did not change during the experiment.

4.2 Preparation of input for simulations

From the transverse emittances as measured in front of the DTL (Figs. 4.1, 4.3) the normalized 100%-rms-emittances of 0.12 and 0.23 mm mrad were extracted horizontally and vertically, respectively. As mentioned in Chap. 4.1 the longitudinal measurement was used to extract the rms-bunch length. A value of 26 mm was found corresponding to a phase spread of 20.7° at 36 MHz and to 62.0° at 108 MHz.

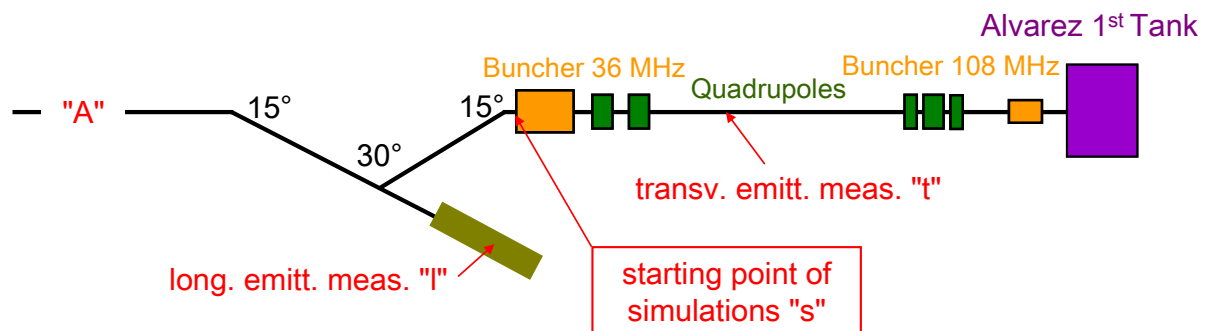


Figure 4.3: Reference points used for the re-construction of the initial phase space distribution as needed for the simulations.

For the 2006 benchmarking campaign more emphasis was put on the re-construction of the initial phase distribution with respect to the 2005 campaign (Chap. 3.3). Additionally, the simulations started at the entrance to the 36 MHz buncher instead of the entrance to the DTL. The re-construction of the initial phase space distribution is complicated by the missing longitudinal information and by the fact that the transverse data and the longitudinal data have been measured at different locations as drawn in Fig. 4.3. These limitations have been dealt with by the following procedure:

1. The measured DTL transmission is very sensitive to the setting of the 36 MHz buncher. Changes of few percent in voltage lead to measurable DTL transmission loss already. Full DTL transmission therefore is a good indicator for longitudinally matched injection into the DTL. The settings during the experiments gave full transmission such that longitudinally matched injection can be assumed.
2. The distance from the location "A" in the beam line to the location "s" where the simulations start is just 0.4 m longer with respect to the distance from "A" to the

location "1" where the bunch length is measured. A virtual transport matrix from "1" to "s" is introduced as a drift with space charge, i.e. neglecting dispersion.

3. At location "t", the measured horizontal and vertical Twiss parameters are used to create Gaussian distribution cuts at 2σ . The obtained two transverse distributions are combined with a longitudinal distribution (Gaussian, cut at 2σ) based on guessed Twiss parameters. Any correlations between coordinates of different planes were assumed to be zero. For the transverse distributions the measured Twiss parameters were taken.
4. The 6D-distribution constructed in "3" is rms-tracked back to location "s" plus additional 0.4 m (see "2"). The tracking includes the space charge forces of rms-equivalent KV-distributions [8].
5. The resulting rms-bunch length is compared to the measured one at "1". In case there is no agreement the procedure must start again at "3" using a different guess on the longitudinal Twiss parameters.
6. In case of agreement the corresponding Twiss parameters at "s" are used as input for the DTL matching routine. The setting for the 36 MHz buncher proposed by the routine is compared to the settings used during the experiments. In case there is no agreement the procedure must start again at "3".
7. In case of agreement the Twiss parameters of the initial distribution at location "s" are assumed to be re-constructed.

The initial phase space at location "s" as re-constructed by this procedure is plotted in Fig. 4.4. It was used for simulations using the DYNAMION code (3476 particles) and the PARMILA code [9] (100000 particles) using a PICNIC Poisson solver. The initial longitudinal 100%-rms-emittance was estimated as 66 deg mrad, referring to 108 MHz and to the relative momentum spread.

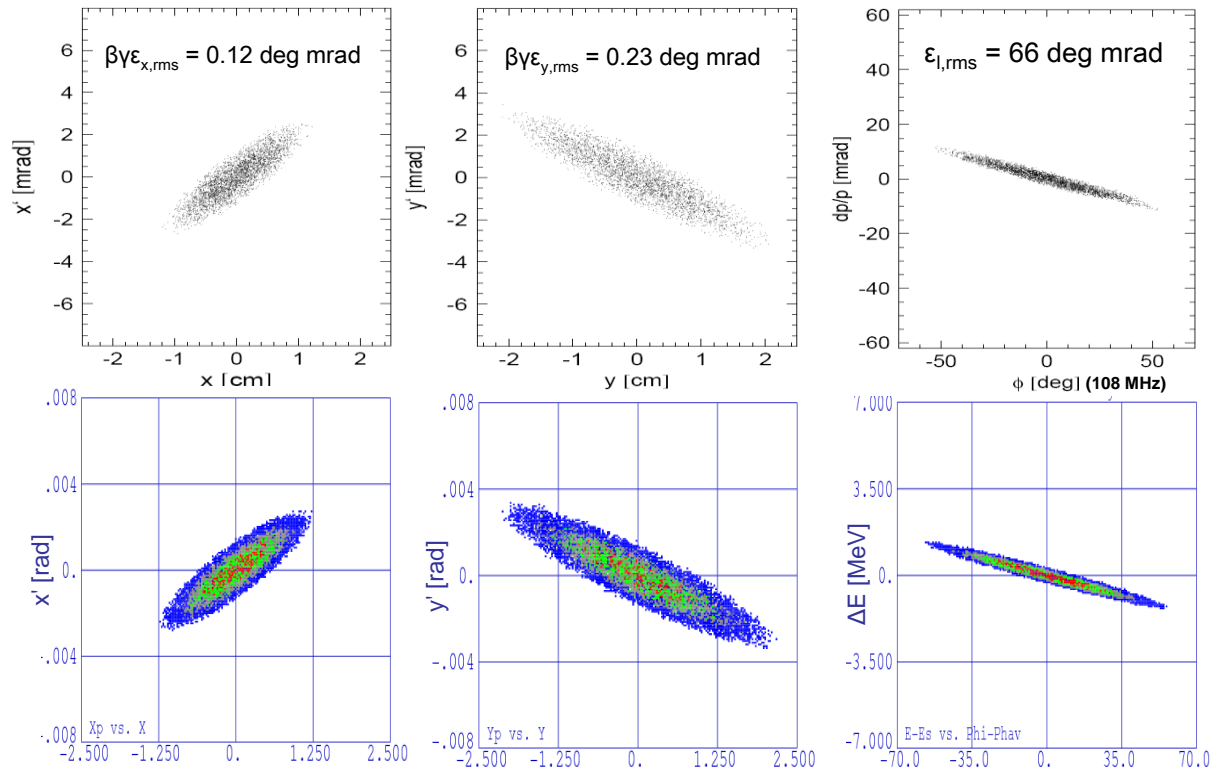


Figure 4.4: Initial phase space distribution at the entrance to the 36 MHz buncher used for DYNAMION (upper) and for PARMILA (lower) simulations. Left: horizontal; centre: vertical; right: longitudinal.

4.2 Comparison of experimental data and simulation result

For all zero phase advances σ_0 ranging from 35° to 90° full beam transmission was measured through the DTL in the experiment as well as in the simulations. Including the measurements performed to check the reproducibility, in total 20 horizontal and vertical phase space distributions behind the DTL were recorded, respectively. In front of the DTL each plane was measured twice for the same reason. Figure 4.5 plots the final phase space distributions obtained from the measurements and from the simulations for two different values of σ_0 .

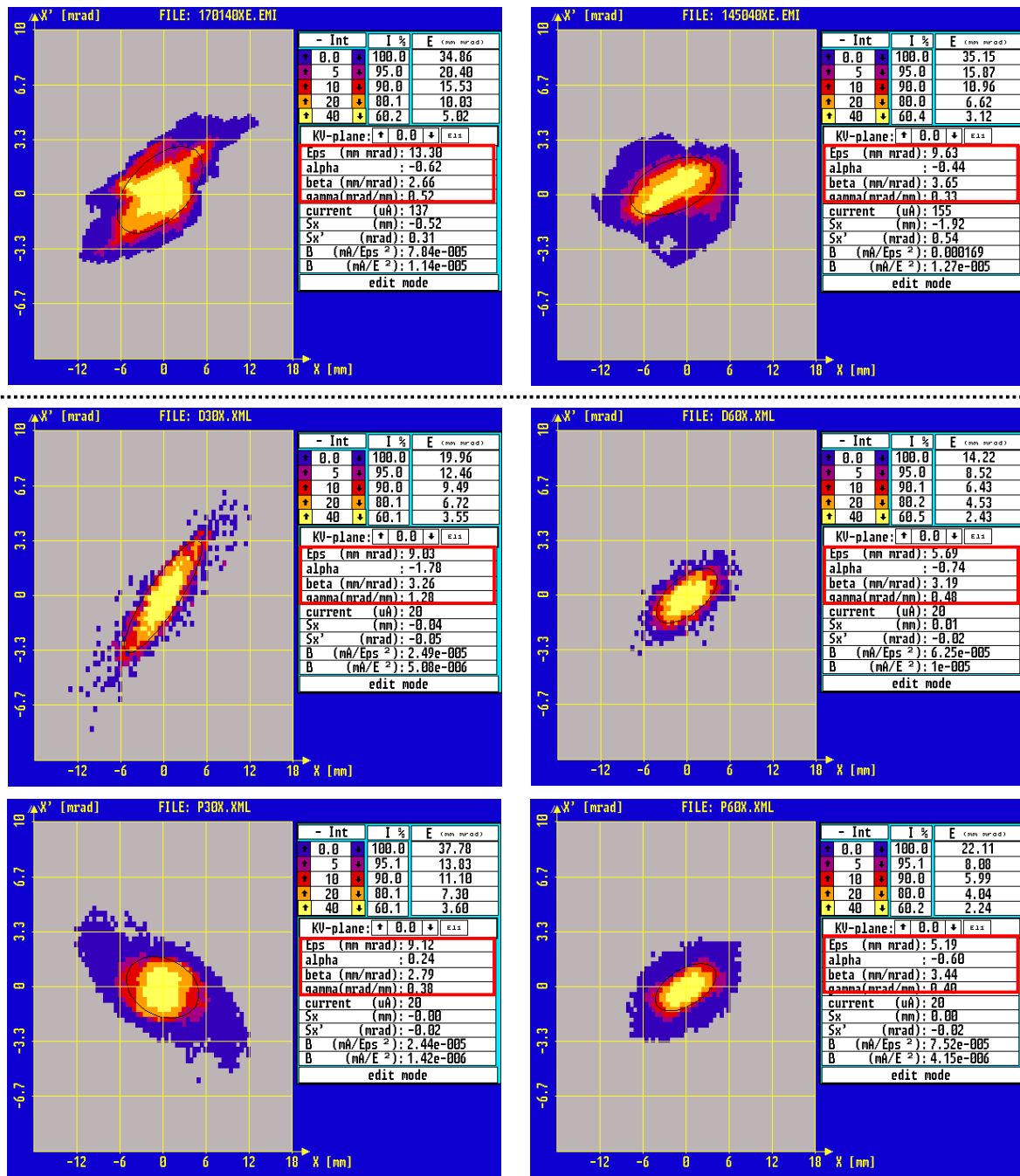


Figure 4.5: Horizontal phase space distributions as measured about 3 m behind the DTL (upper) and simulated at the exit of the last drift tube using DYNAMION (centre) and PARMILA (lower). Left: $\sigma_0 = 35^\circ$; right: $\sigma_0 = 60^\circ$. The Twiss parameters corresponding to 100% of the total intensity are highlighted in red.

The simulations were evaluated in the same way as in the 2005 benchmarking campaign (Chap. 3.4). It must be mentioned that the location of the measurement set-up is about 3 m behind the DTL, while the simulations have been evaluated at the end of the final drift tube of the DTL. This short drift does not cause any emittance growth. For all σ_0 the simulations delivered final phase space distributions that are similar to ellipses, while the measured distributions for very low or very high σ_0 give inhomogeneous shapes as seen for the $\sigma_0 = 35^\circ$ case at the left of Fig. 4.5. Additionally, the simulated shapes at phase advances between about 45° to 65° look quite similar for the two codes, while for instance in case of 35° even

the orientations of the horizontal distributions are of opposite sign for the two codes. Concerning beam transmission both codes gave full DTL transmission as seen in the experiment.

4.2.1 Comparison of 100%-rms-emittance data

From the experimental and the simulated data the 100%-rms-emittances have been extracted. For the accuracy of the experimental data points a value of 10% was assumed (Chap. 3.2). The results are plotted in Fig. 4.6a as function of the zero current phase advance σ_0 along the DTL. Averaged transverse emittances, i.e. the mean values of horizontal and vertical emittances, are presented in Fig. 4.6b.

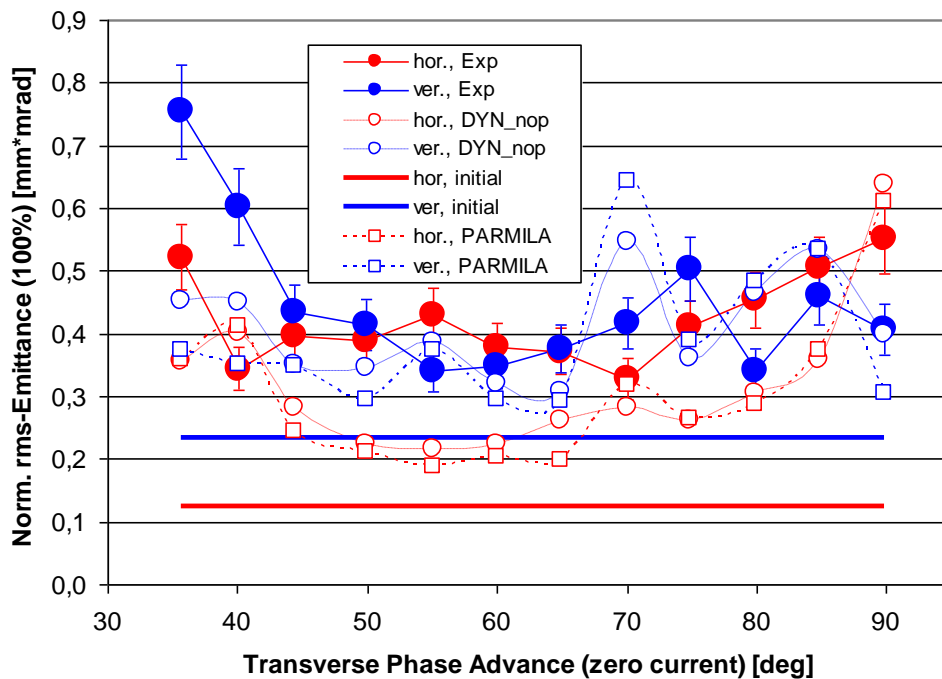


Figure 4.6a: Horizontal and vertical 100%-rms-emittances at the DTL exit as function of the transverse zero current phase advance σ_0 .

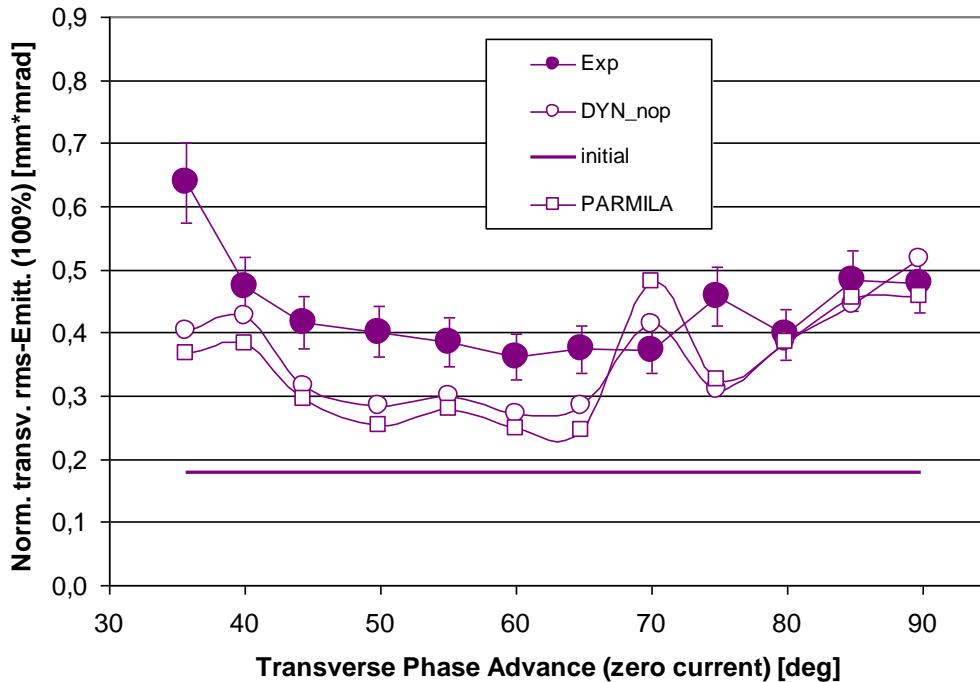


Figure 4.6b: Mean value of horizontal and vertical 100%-rms-emittances at the DTL exit as function of the transverse zero current phase advance σ_0 .

The measured horizontal and vertical emittances show a broad minimum at zero current phase advances of about 60° , although a scattering of the individual data points around this general behaviour is observed. This tendency is also seen in the simulations, although the scattering is less with respect to the measurements. The agreement between the simulation codes is very good for intermediate phase advances but differences are observed for low and for high phase advances. The differences between the codes seem slightly stronger in the vertical plane; especially for $\sigma_0 < 45^\circ$ they are significant. Both codes predict a dominant peak of the vertical emittance at 70° .

As already observed in the 2005 benchmarking campaign (Chap. 3.5.1), the simulated 100%-rms-emittances are lower with respect to the measured ones (with exception of the vertical plane for $\sigma_0 > 75^\circ$). Additionally, the simulated vertical emittances are generally larger than the horizontal emittances, while this was not observed in the experiment, where for several cases an emittance exchange between the two transverse planes occurred. The significant vertical peak at 70° was not seen in the experiment.

It might be argued if the observed difference of measured and simulated emittances is due to a wrong assumption on the initial longitudinal emittance. Accordingly, simulations have been performed using initial longitudinal emittances of 7, 37, and 112 deg mrad as well for the 45° case. The transverse emittances differed by 5% at maximum. This observed independence from the initial longitudinal emittance is reasonable since the initial bunch length does effectively not change as long as the rules for phase space re-constructions motivated in Chap. 4.2 are applied. It is the initial bunch length that enters into the space charge forces.

As already mentioned in Chap. 3.5.1 the simulations assume a machine without any errors. Such errors generally drive an additional emittance growth.

4.2.2 Comparison of measured 90%-rms-emittance data with simulated 95%-rms-emittances

The general motivation for evaluating fractional emittances is given in Chap. 3.5.2 and the procedure of the evaluation itself is presented in Chap. 3.2. As already done in the 2005 benchmarking campaign (Chap. 3.5.2), the measured 90%-rms-emittances are compared to the simulated 95%-rms-emittances. The corresponding plots of these emittance values as function of the transverse zero current advance σ_0 are presented in Fig. 4.7a (horizontal and vertical values separately) and Fig. 4.7b (average of horizontal and vertical values).

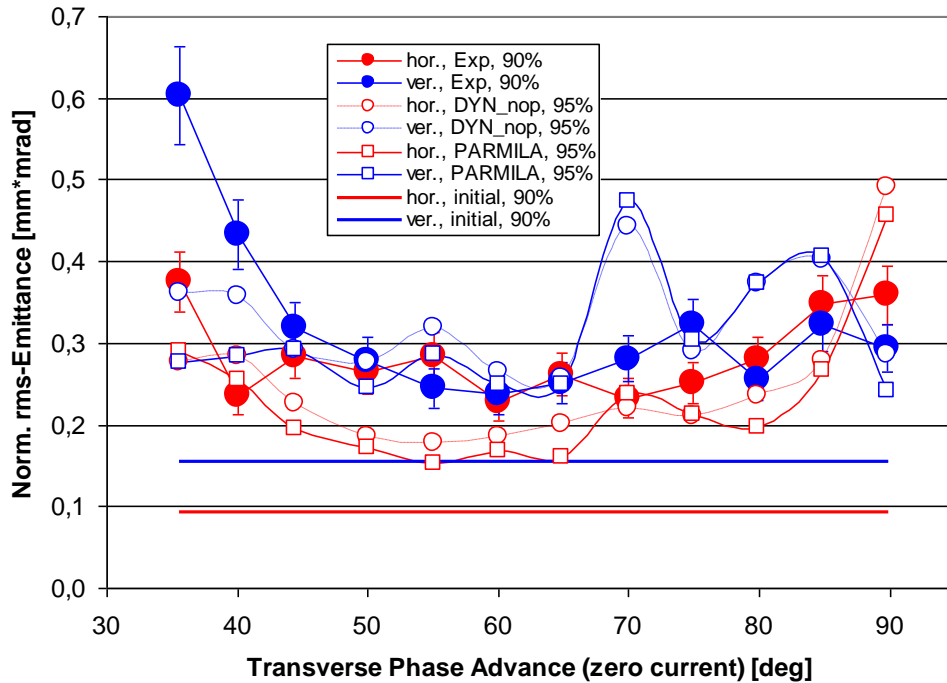


Figure 4.7a: Horizontal and vertical rms-emittances at the DTL exit as function of the zero current phase advance σ_0 . The experimental values refer to 90% of the total intensity while the simulated values refer to 95% of the particles.

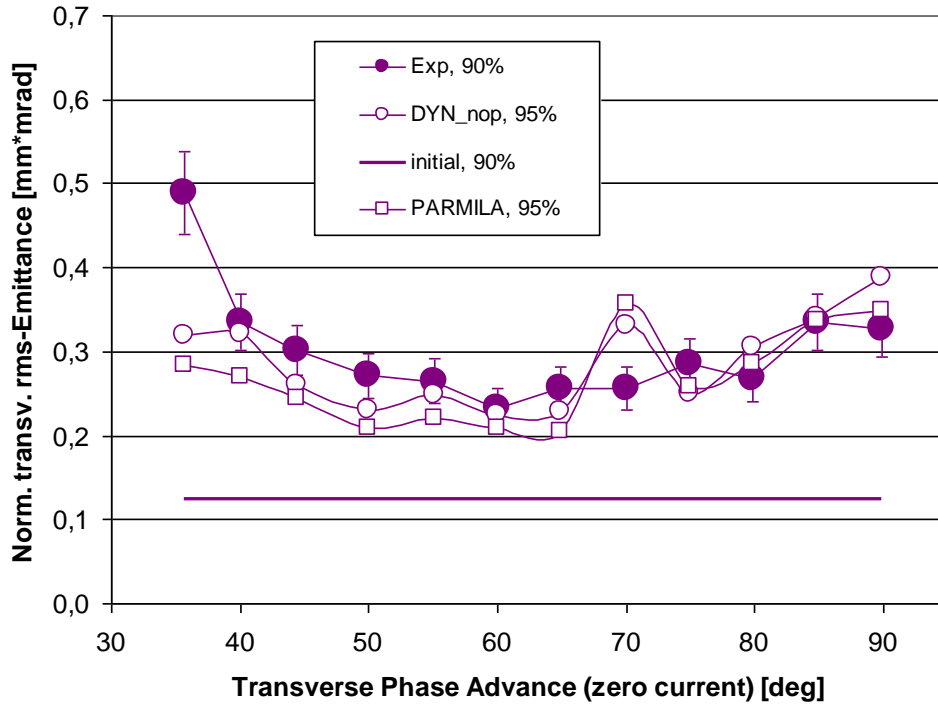


Figure 4.7b: Mean value of horizontal and vertical rms-emittances at the DTL exit as function current phase advance σ_0 . The experimental values refer to 90% of the total intensity while the simulated values refer to 95% of the particles.

The quantitative behaviour of the curves for fractional emittances is the same as for the case of the 100%-rms-emittances (Chap. 4.2.1). However, the differences between measurements and simulations are significantly reduced if fractional emittances are compared. The simulated horizontal values are still too low with respect to the measured once. The vertical values instead seem to scatter around the same general behaviour, although for higher phase advances the simulations predict slightly higher emittances. For the fractional rms-evaluation the vertical peak at 70° remains, indicating that it is not due to an extended halo comprising just a tiny fraction of the total intensity but that rather a major part of the beam is affected.

Except for the strong enhancement at 70° , the averaged values of horizontal and vertical emittances agree well ($\sigma_0 < 65^\circ$) to excellent ($\sigma_0 > 65^\circ$) among experiment, DYNAMION- and PARMILA simulations. This good agreement was observed already in the 2005 campaign (Chap. 3.5.2).

4.2.3 Mismatch

As mentioned in the introduction to Chap. 4.1, the campaign suffered from mismatch between the injected beam rms-Twiss parameters and the periodic solution at the entrance to the DTL. The mismatch arose due to the fact that the matching routine was fed using the wrong initial longitudinal rms-Twiss parameters. Although this does not harm the main goal of the campaign, i.e. the experiment vs. simulation benchmarking, it has an impact on the emittance growth along the DTL. This growth comprises two components: the first being intrinsic due to the transverse focusing along the DTL and the second one being caused by matching conditions that depend on the chosen transverse phase advance σ_0 .

The amount of mismatch for each σ_0 was estimated using the DYNAMION simulations by evaluating the simulated phase space distributions at the entrance to the DTL and comparing their rms-Twiss parameters with the periodic solution for this specific σ_0 . Figure 4.8 depicts phase space distributions right in front of the DTL as obtained from DYNAMION simulations. The ellipses corresponding to the beam rms-Twiss parameters and to the rms-matched solution of the DTL are drawn as well. From these two Twiss parameters for each plane the resulting mismatch parameter M is calculated using the definition given in [10].

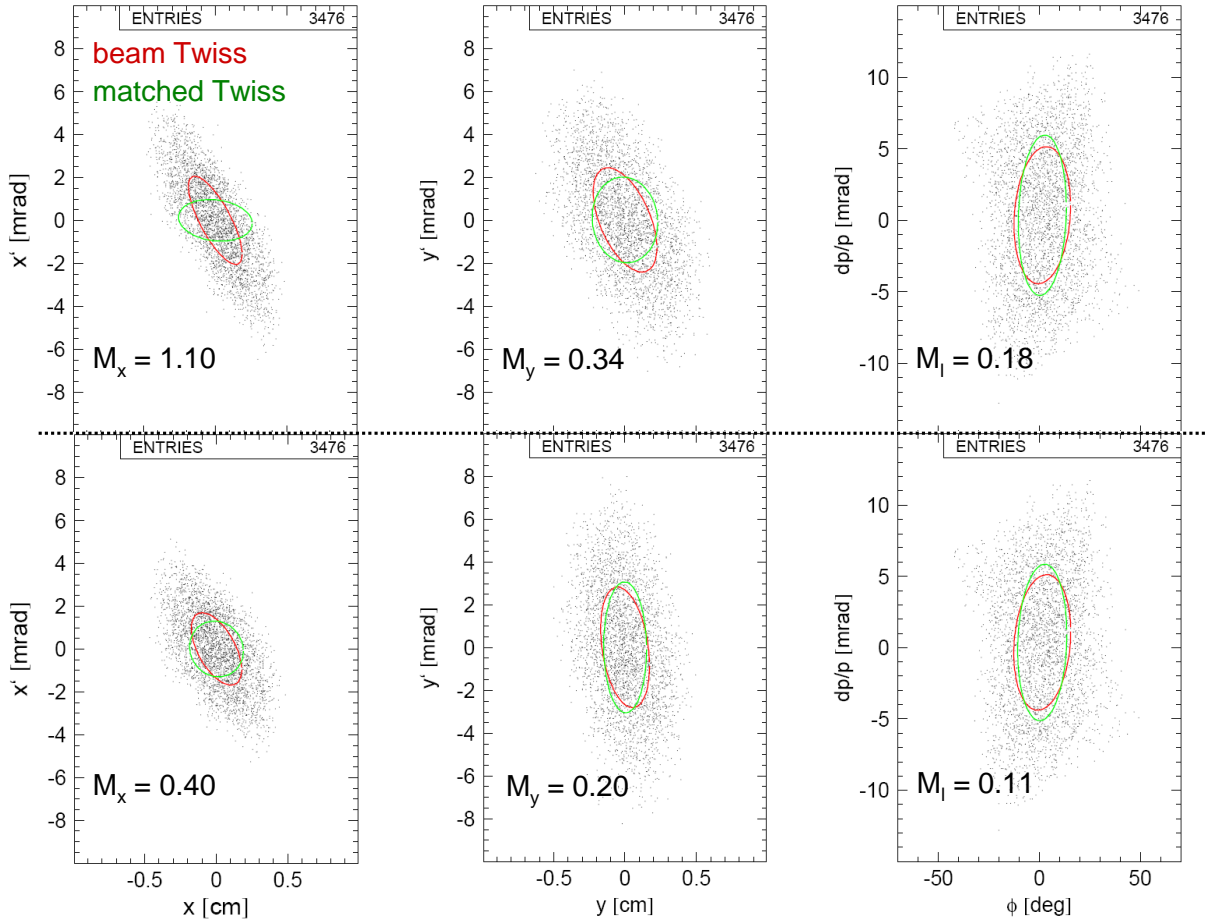


Figure 4.8: Phase space distributions from DYNAMION simulations at the entrance to the DTL for different zero current phase advances σ_0 (upper: 35° ; lower: 60°). The ellipses correspond to the rms-Twiss parameters of the distributions (red) and the rms-matched injection into the DTL (green).

The mismatch parameters in the three planes were calculated for all phase advances applied during the experiment. They are plotted as function of σ_0 in Fig. 4.9. It turned out that the transverse mismatch varied significantly with the phase advance, while the longitudinal remained constant. The low longitudinal mismatch for all values of σ_0 confirms the sensibility of the machine setting with respect to correct longitudinal injection into the DTL. Higher longitudinal mismatches could have been detected immediately during the experiment by the occurrence of transmission losses. This observation together with the fact that the longitudinal mismatch is mainly controlled by the 36 MHz buncher, underlines the relevance of including this buncher setting into the method to re-construct the initial phase space distribution for the simulations (see Chap. 4.2).

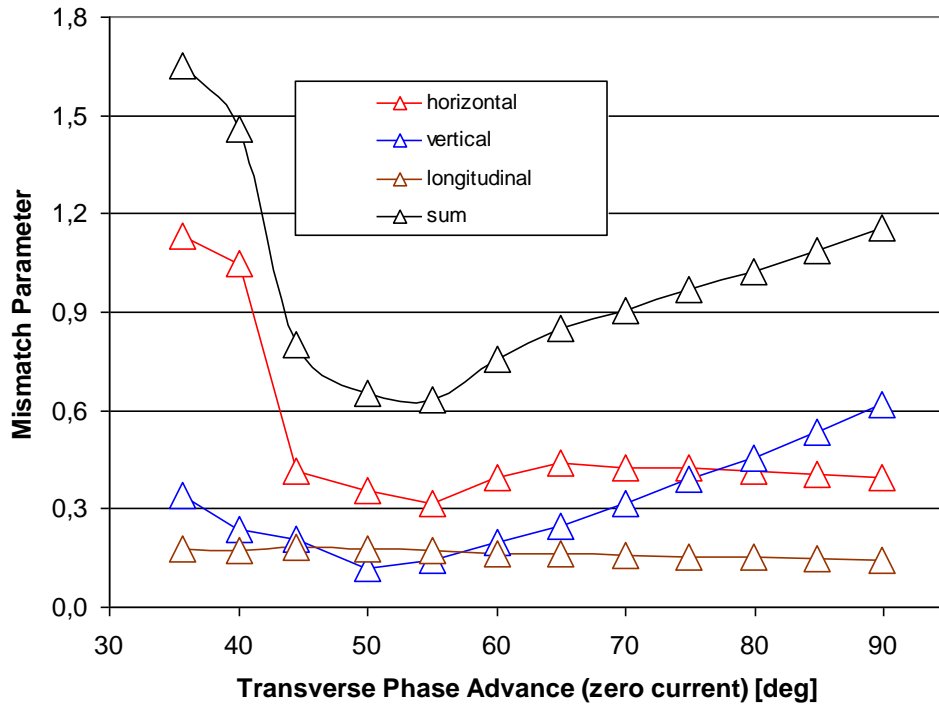


Figure 4.9: Mismatch between beam rms-Twiss parameters and the Twiss parameters for the rms-matched injection into the DTL as function of the current phase advance σ_0 .

5 Summary and conclusion

Extensive benchmarking studies on transverse rms-emittance growth along an Alvarez DTL have been performed during two different campaigns. The first one in 2005 investigated the DTL exit rms-emittance as function of the final DTL energy. Experiments were compared with DYNAMION simulations using 3D particle-particle interaction and 1500 particles.

The second campaign in 2006 aimed for the study of the final DTL rms-emittance as function of the transverse focusing strength along the DTL. These results were compared with DYNAMION simulations using 3476 particles. Additionally, PARMILA simulations using a PIC solver using 100000 particles were performed.

Both benchmarking campaigns revealed good agreement on averaged transverse emittances between codes and experiment in case that experimental 90%-rms-emittances are compared with simulated 95%-rms-emittances. For comparison of 100%-rms-emittances the experimental values significantly exceed the predictions of simulations. The agreement between the two codes is excellent for fairly matched injection into the DTL. Notable differences between the codes occur for poorly matched injection.

Future efforts aim for the extension of longitudinal diagnostics in front of the DTL from rms-bunch lengths to full phase space distributions. This will allow for measurements with improved matching to the periodic DTL.

Simulations including alignment- and machine errors might help in understanding the observed difference between measured and simulated 100%-rms-emittances. Benchmarking has been done so far with the DYNAMION and the PARMILA codes. Other codes should be

included into these efforts. First simulations with PARTRAN just have been started at CEA/Saclay [11].

Acknowledgement

We acknowledge the support of the European Community-Research Infrastructure Activity under the FP6 “Structuring the European Research Area” programme (CARE, contract number RII3-CT-2003-506395)

Literature

- [1] *FAIR Baseline Technical Report*, Vol. 2, GSI Darmstadt, Germany, p. 335, (2006).
- [2] W. Barth, L. Dahl, L. Groening, J. Glatz, S. Richter, S. Yaramyshev, *Development of the UNILAC towards a Megawatt Beam Injector*, Proc. of the XXII Linac Conf., Lübeck, Germany (2004).
- [3] L. Groening and W. Barth, *Measurements and Simulations on the Beam Brilliance in the Universal Linear Accelerator UNILAC at GSI*, Proc. of the XXI Linac Conf., Gyeongju, Korea, (2002).
- [4] P. Forck, F. Heymach, T. Hoffmann, A. Peters, P. Strehl, *Measurement of the six Dimensional Phase Space at the New GSI High Current Linac*, Proc. of the XX Linac Conf., Monterey, U.S.A., (2000).
- [5] S. Yaramyshev, W. Barth, L. Groening, A. Kolomiets, T. Tretyakova, *Development of the versatile multi-particle code DYNAMION*, Nucl. Instrum. & Methods in Phys. Res. A **558**, 1, (2006).
- [6] L. Groening, W. Barth, I. Hofmann, *Status of Beam Dynamics Experiment at the UNILAC*, Annual HIPPI meeting 2004, <http://hippi04.web.cern.ch/hippi04/index.htm>.
- [7] L. Groening, http://www-linux.gsi.de/~lgroenin/bd_unilac/HSI/Alvarez_Matching.html.
- [8] Th. Wangler, *Rf Linear Accelerators*, John Wiley & Sons Inc., p. 278, (1998).
- [9] J.H. Billen and H. Takeda, *PARMILA Manual*, Report LAUR-98-4478, Los Alamos, 1998 (Revised 2004).
- [10] Th. Wangler, *Rf Linear Accelerators*, John Wiley & Sons Inc., p. 217, (1998).
- [11] D. Uriot, CEA/Saclay, private communication.